ACS OMEGA

Open Access

http://pubs.acs.org/journal/acsodf

Article

Keratose Self-Cross-Linked Wound Dressing for Iron Sequestration in Chronic Wounds

Anastasia Anceschi, Alessia Patrucco,* Parag Bhavsar, Marina Zoccola, Mirko Tessari, Luca Erbazzi, and Paolo Zamboni

Cite This: *ACS Omega* 2023, 8, 30118−30128

Read Online

ACCESS | Metrics & More | Article Recommendations

ABSTRACT: Chronic wound diseases affect a large part of the world population, and therefore, novel treatments are becoming fundamental. People with chronic wounds show high iron and protease levels due to genetic disorders or other comorbidities. Since it was demonstrated that iron plays an important role in chronic wounds, being responsible for oxidative processes (ROS generation), while metalloproteinases prevent wound healing by literally "eating" the growing skin, it is crucial to design an appropriate wound dressing. In this paper, a novel bioactive dressing for binding iron in chronic wounds has been produced. Wool-derived keratose wound dressing in the form of films has been prepared by casting an aqueous solution of keratoses. These films are water-soluble; therefore, in order to increase their stability, they have been made insoluble through a thermal cross-link treatment. Fourier transform infrared (FTIR), differential scanning calorimetry (DSC), and thermogravimetric analyzer (TGA) analyses clarified the structure and the properties of the keratose wound dressing films. The capability of this new biomaterial in iron sequestration has been investigated by testing the adsorption of Fe^{3+} by inductively coupled plasma-optical emission spectrometry (ICP-OES). The results suggest that the keratose cross-linked films can adsorb a large amount of iron (about 85% of the average amount usually present in chronic wounds) following pseudo-second-order kinetics and an intraparticle diffusion model, thus opening new perspectives in chronic wound care. Furthermore, the QSAR Toolbox was applied for conducting *in silico* tests and for predicting the chemical behavior of the C-Ker-film. All of the data suggest that the keratose bioactive dressing can significantly contribute to wound healing by mechanisms such as iron depletion, acting as a radical scavenger, diminishing the proteolytic damage, acting as a substrate in place of skin, and, finally, promoting tissue regeneration.

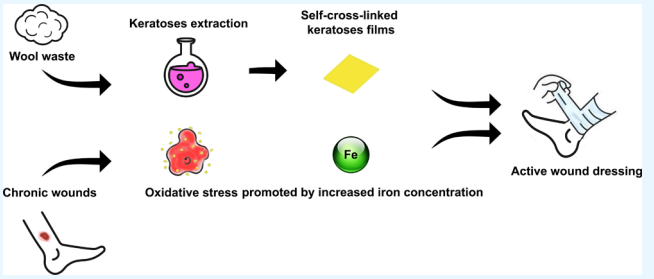

1. INTRODUCTION

Global skin and subcutaneous diseases have increased rapidly over 10 years, with a prevalence of 605 036 000 in 2015 compared to 492 883 000 in 2005 based on global, regional, and national data from over 195 countries.[1] Thus, understanding and addressing the challenges in treating chronic wounds will increase clinical outcomes, improve the quality of life of patients, and reduce healthcare costs.

Chronic wounds are ulcers that do not progress through the healing process promptly, and they generally occur in adults with vascular disease.[2] One of the most critical factors that affect the normal healing process of the wound is diabetes. Particularly, diabetes mellitus is one of the frequent metabolic disorders characterized by abnormal glucose metabolism.[3] Elevated blood glucose levels are responsible for many complications, including nephropathy, cardiomyopathy, and skin ulcers.[4] Currently, the most significant complication affecting diabetic patients is diabetic wounds that can quickly develop into chronic ulcers.[3] These kinds of wounds are mostly attributed to chronic venous insufficiency, followed by critical limb ischemia, prolonged pressure, neuropathy, or mixed etiology. Ulcers last on average 12−13 months, recur in up to 60−70% of patients, and can lead to loss of function, decreased quality of life, or death following infective complications or amputations.[5] Traditional healthcare treatments such as controlling blood glucose, surgical debridement removal, skin transplantation, and hyperbaric oxygen therapy have a limited therapeutic effect on the healing of these kinds of ulcers. Since these treatments require a long time, it has tremendous psychological and physical impacts on a patient.[2]

Basically, wound healing is a complex dynamic process that starts when the skin and tissue integrity are affected.[6] The normal healing process can be divided into hemostasis,

Received: April 13, 2023
Accepted: July 6, 2023
Published: August 8, 2023

inflammation, proliferative, and remodeling phases. Immediately after skin or tissue damage, hemostasis occurs, and numerous reactions initiate the healing process. In this phase, the predominant cells at work are phagocytic cells, such as neutrophils and macrophages.[7] The healing process fails to proceed through the usual phases in chronic wounds. Specifically, chronic wounds often prolong the inflammation phase with an excessive level of proinflammatory cytokines, proteases, and ROS, and senescent cells are often absent and dysfunctional.[8] Quite recently, it has been shown how the lack of switch of macrophages from inflammatory phenotype to regenerative phenotype is essential for the typical sequence of the healing process.[9]

Generally, proteases are regulated by their inhibitors, but in chronic wounds, protease levels exceed their respective inhibitors, leading to the degradation of growth factors and their receptors. The proteolytic destruction of extracellular matrix proteins prevents the wound from moving into the proliferative phase and attracts more inflammatory cells, thus amplifying the inflammation cycle.[10] In chronic wounds, oxidative stress is caused by an imbalance of ROS, resulting in a high level of potentially oxidant free radicals such as hydroxyl radicals (°OH).[11] In venous leg ulcers, the more common variety of chronic wounds, venous hypertension is transmitted to the microcirculation, facilitating the extravasation of red blood cells from the capillary bed. Erythrocytes are phagocyted by the interstitial macrophages, and iron is incorporated into ferritin and hemosiderin proteins.[12] Iron released from hemoglobin or other iron−sulfur proteins plays an important role in enabling oxidative stress. Although iron is the most abundant and essential transition metal in the human body, its toxicity lies in the ability to undergo a cycle of oxidative and reduction reactions resulting in the generation of several free radicals.[13] Through the Fenton reaction, these radicals can initiate a sequence of biological injuries, prolonging the oxidative stress.[14]

Meyer and co-workers proposed the first hypothesis that iron could be a significant factor in venous ulcers. The "statis" pigmentation that commonly surrounds venous ulcers is the result of the deposition of hemosiderin from red blood cell disruption.[15] Ackerman et al. found out that brown pigmentation is related to the increase of dermal iron deposition, playing an important role in perpetuating the damage of tissues by carrying forward the local inflammation.[16] Recent studies have demonstrated the role of iron as an oxidative agent in chronic wounds.[17−19] The local anoxia, the inflammation, and the incorrect activation of neutrophils are responsible for the generation of free radicals, which can induce continuing tissue damage.[17,20] Finally, the relative instability of iron is sometimes due to a gene mutation that can increase the susceptibility to the development of venous leg ulceration.[21]

Since it was demonstrated that iron plays an important role in chronic wound healing and skin repair is an intricate biochemical event, it is crucial to design an appropriate wound dressing.[22] An ideal dressing should remove the excess of exudate, promote autolytic debridement, and allow adequate breathability. Furthermore, it should be adhesive, flexible, and easy to apply or remove.[23] Nowadays, nurses and doctors usually clean the wound from the debridement and then apply an appropriate care material. Several materials such as films, gauze, hydrogels, hydrocolloids, and alginates, as well as silver-based dressing have been used. Several techniques have been applied for this purpose, such as film-casting, electrospinning, freeze-drying, salt leaching, and emulsion based on synthetic macromolecules or the material of natural origin.[24−27]

Recently, bio-based polymers have largely attracted the scientific community's interest. Above all, the most attractive in terms of biocompatibility and biodegradability are polysaccharides and proteins.[25,28] They allow reaching the highest level of biomimicry, simulating the native biological and physical−chemical features. In particular, protein-based biopolymers are gaining attention due to their natural antimicrobial, anti-inflammatory, cell proliferative, and angiogenic effects. All of these issues are favorable for the healing process.[22] Several proteins have been investigated as possible building blocks for synthesizing biopolymers, and various dressing architectures have been exploited. One of the most investigated proteins is collagen. Several collagen-based wound dressings, in the form of hydrogels, electrospun fibers, or scaffolds, have been applied for wound treatment, showing promising results.[29−32] Other authors report that many processing techniques with the consequent fabrication of multiple active materials can be obtained using silk fibroin.[22,33] Silk proteins are produced in the epithelial cells of various arthropods, such as spiders and silkworms, and their specific structure confers high toughness and elasticity to these materials.[34]

Another important protein is keratin. It is produced in the epithelial cells of mammals, birds, reptiles, and humans.[35] It is the structural component of wool, nails, horn, feathers, and hair. Wool keratins have received significant interest among the available sources of keratin due to their higher extraction yields and structural advantages. Additionally, it was reported that wool keratin is a promising candidate in biological and pharmaceutical fields because it has arginine−glycine−aspartic acid and leucine−aspartic acid−valine groups in its amino acid sequence, which can promote cell adhesion.[36] Indeed, wool keratin film and sponges have been demonstrated to provide better adhesion for fibroblasts and to be suitable for long-term cell cultivation.[37]

The keratin must be extracted by wool, and this extraction can be performed using techniques such as reduction, sulfitolysis, alkali hydrolysis, enzymatic hydrolysis, ionic liquid treatment, microwave irradiation, steam explosion, and oxidation.[38−40] The oxidation method of extraction allows one to obtain the soluble fraction of keratin, keratoses, breaking the disulfide bonds and converting some thiol in cysteic acids.[41] Typically, keratoses are used alone or in blends with other polymers for making fibers, films, sponges, and hydrogels for the biomedical field.[41,42] More specifically, many reports demonstrate keratin's potential, mainly in the form of hydrogels for drug delivery, wound healing, nerve regeneration, dental implants, and vascular smooth muscle differentiation.[43] In addition, keratin can bind metals and its properties can be tailored, resulting in biomaterials with different mechanical, swelling, and chelating properties.

For all of these reasons, the use of keratoses to prepare bioactive wound dressing has been explored in this paper.

2. RESULTS AND DISCUSSION

In order to obtain the soluble fraction of keratin (keratoses), wool was subjected to oxidative extraction. Briefly, wool was first treated with peracetic acid, which oxidizes cysteine to cysteic acid, giving the keratin the soluble property. After that, the solution was filtered and rinsed with MilliQ water. The

https://doi.org/10.1021/acsomega.3c02525
ACS Omega 2023, 8, 30118−30128

oxidized wool was treated with tris(hydroxymethyl)-aminomethane (TRIS) for 2 h at 37 °C. Then, the solution was filtered and the purification process took place through the use of a dialysis tube in a distilled water-circulated system. The obtained keratoses were then freeze-dried and properly stored for future analysis and preparation. The yield of extraction was about 31% (% w/w). Then, the film was prepared by dispersing an appropriate amount of keratoses in water, and the viscous solution achieved was poured into a polypropylene mold and dried at 20 °C (Ker-film).

2.1. Thermal Analysis. Since the Ker-film is water-soluble, a thermal treatment has been performed to obtain cross-linking reactions to stabilize the wound dressing to the wound exudate environment for the usage time (*i.e.*, 7 days). Thus, DSC was carried out to better understand the cross-linking reaction, and the results are reported in Figure 1. Basically, the Ker-film was heated to 180 °C and cooled to 30 °C, and then, the sample was subjected to a second thermal cycle.

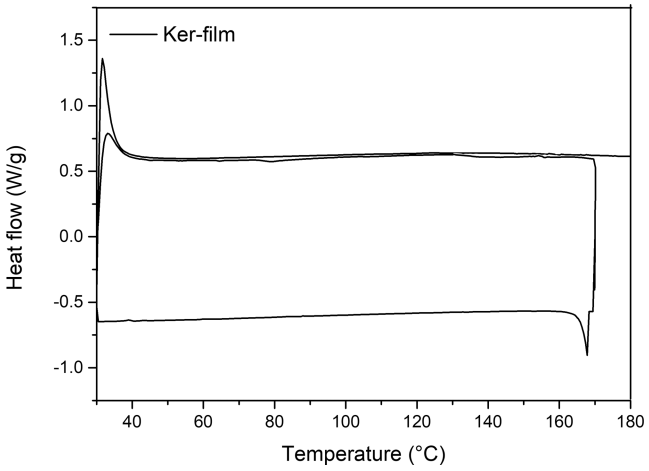

Figure 1. DSC of the Ker-film.

During the first ramp, an exothermic process occurs between 70 and 180 °C associated with the cross-linking reaction. An isothermal step of 30 min was performed during the DSC analysis in order to identify the correct duration of the heating treatment. It was found that 30 min can be an enough timeframe to guarantee the complete self-cross-linking reaction of the Ker-film. Indeed, in the second heating ramp, no further exothermic phenomena take place and, consequently, the cross-linking reaction can be considered concluded. Thus, the film was cross-linked at 170 °C in an oven to make the film insoluble (C-Ker-film). In Figure 2, the visual appearance of Ker-film (a) and C-Ker-film (b) is reported. After the thermal treatment, no evident morphological changes can be detected; only a slight color variation can be seen.

The thermal stability of the C-Ker-film was explored using a thermogravimetric analyzer (TGA) in a range of temperatures from 30 to 800 °C in an inert atmosphere. In Figure 3, the TGA (a) and the first derivative, DTG, (b) of the C-Ker-film are reported. For comparison, the TGA of the Ker-film is also reported.

Two degradation steps can be distinguished in the thermal degradation of the Ker-film and the C-Ker-film. The first one starts immediately and finishes at about 130 °C. This stage can be associated with the evaporation of the water absorbed, and the weight loss is about 8%. The main degradation step for the

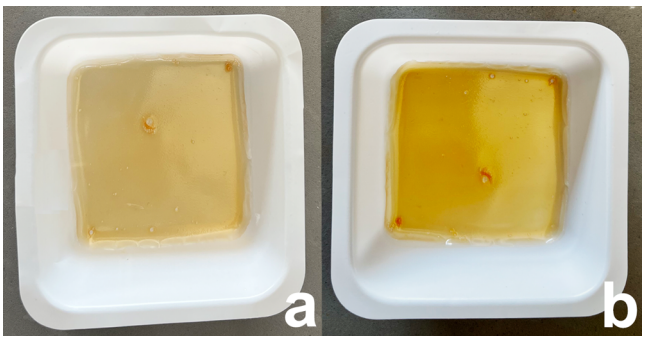

Figure 2. (a) Visual appearance of the Ker-film. (b) Visual appearance of the C-Ker-film.

Ker-film and the C-Ker-film starts at 210 °C and finishes at 470 °C. Although the degradation temperature is the same for both samples, the degradation pathways followed by the two samples have some differences, as shown by the DTG analysis in Figure 3b. The degradation rate for the two samples shows some differences probably related to the presence of cross-linking bonds along the C-Ker-film protein chains. Presumably, the chemical nature of the cross-linking bridge strongly influences the degradation pathway. The new bonds are probably weaker than the peptide bonds and consequently modify the decomposition pathways of the C-Ker-film. Furthermore, these bonds favor the volatilization reactions, causing a faster and more significant weight loss. Indeed, during the main decomposition step, the Ker-film loses 72% of its initial weight, whereas the C-Ker-film loses 76%.

2.2. Scanning Electron Microscopy (SEM) Analysis. In order to investigate the differences in the morphology of the Ker-film and the C-Ker-film, a SEM analysis was performed, and the results are reported in Figure 4.

In Figure 4a, the Ker-film, which is soluble in water, shows a very smooth surface and no aggregates are present, indicating a complete solubilization of the keratoses and no precipitation during the casting process. Regarding the C-Ker-film, in Figure 4b, it is possible to see that the surface morphology is wrinkled and rough. This can be due to the fact that the water-insoluble films are composed of keratose molecules that reassemble their structure as a result of the cross-linking reaction, causing changes in the surface structure morphology.

2.3. Water Stability. The water stabilities of Ker-film and C-Ker-film were investigated by dipping the samples in water for different contact times and evaluating the weight loss. As expected, the untreated keratoses film was entirely dissolved in water after a few minutes of contact time. On the contrary, the thermally treated film showed greater water stability, and the obtained results are shown in Figure 5a. Indeed, after one week, the C-Ker-films showed 6% weight loss.

In addition, further details about thermal stability were obtained by UV−vis spectroscopy. The Ker-film is soluble in water, and its solution generates an absorption band at 260 nm. Thus, to verify the water stability of the C-Ker-film, the presence of the soluble fraction released in water was investigated by analyzing the water suspension after different contact times at 260 nm. The resulting spectra are almost flat, and only after one week can it be possible to detect some soluble residues of keratoses, as shown in Figure 5b.

Furthermore, a swelling test was performed. Swelling is an essential property for studying the water-holding ability and permeability of new materials and foreseeing its behavior *in*

https://doi.org/10.1021/acsomega.3c02525
ACS Omega 2023, 8, 30118−30128

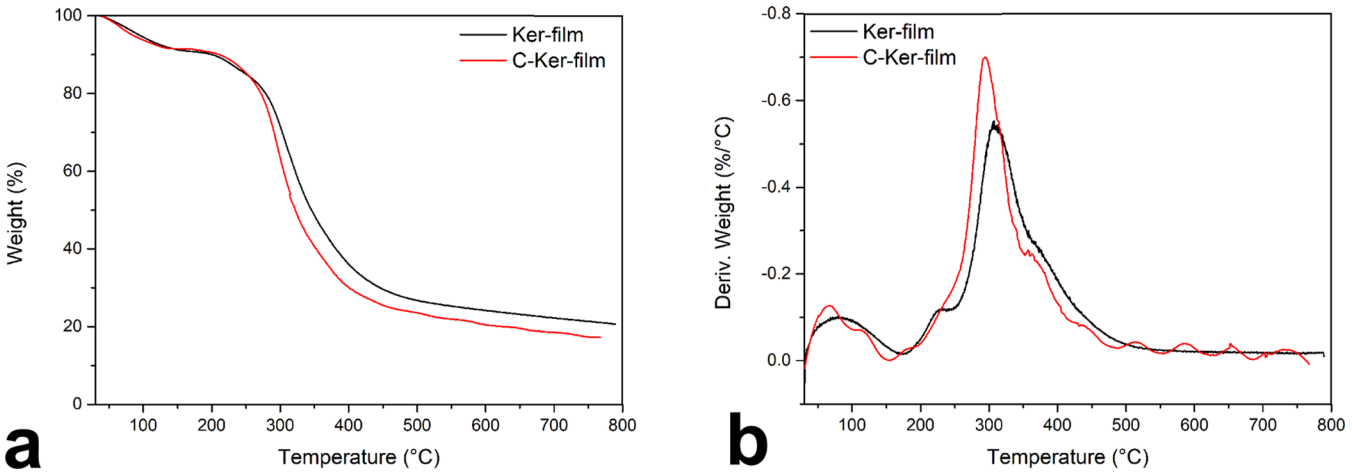

Figure 3. (a) TGA of the Ker-film and the C-Ker-film. (b) DTG of the Ker-film and the C-Ker-film.

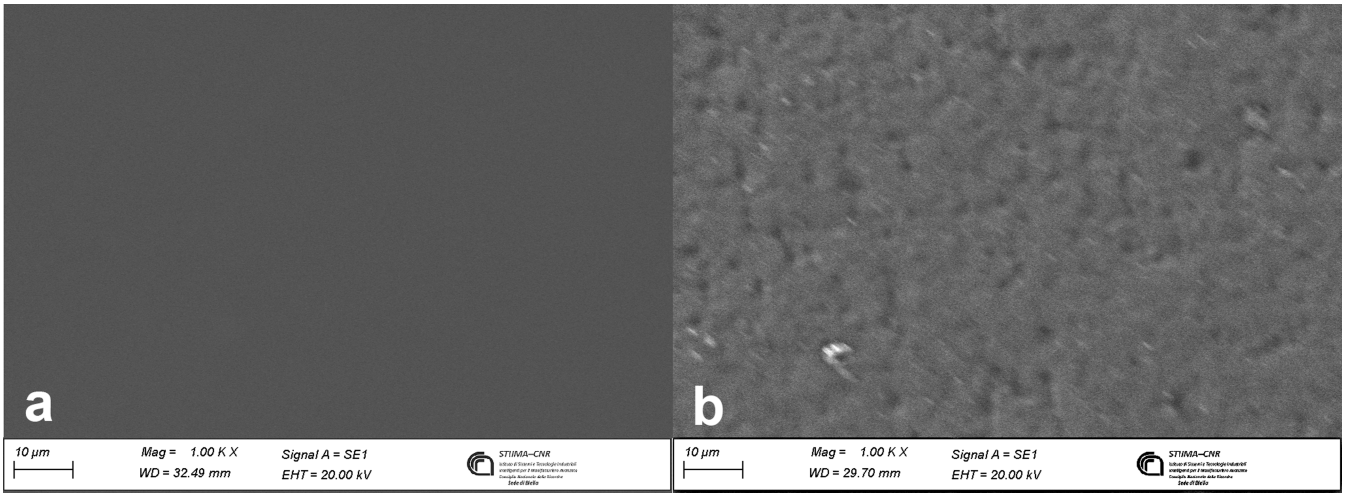

Figure 4. (a) Micrograph of the Ker-film surface; (b) micrograph of the C-Ker-film surface.

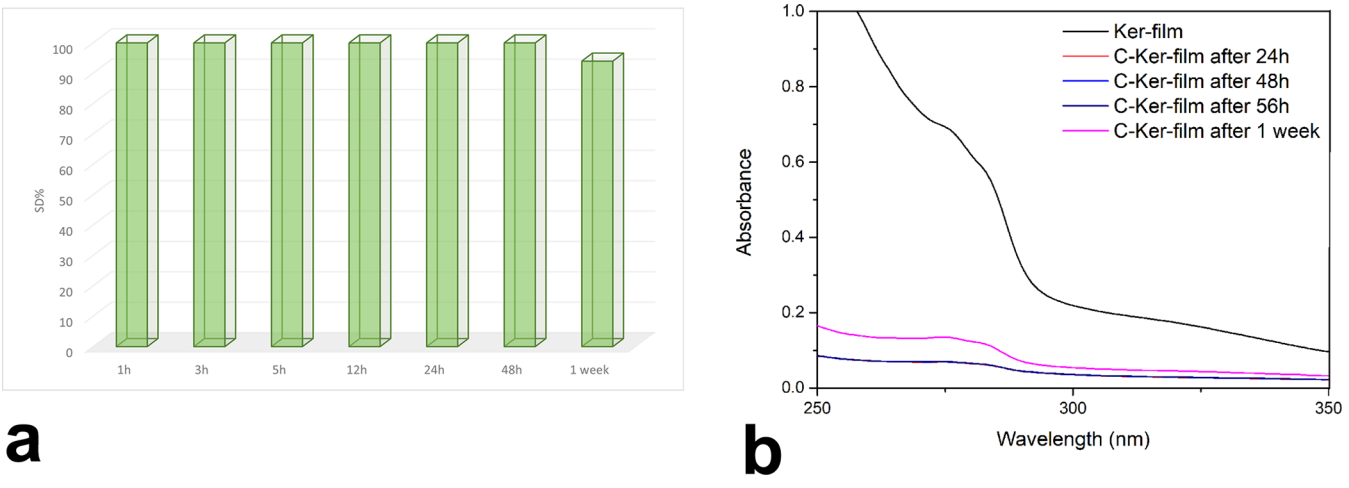

Figure 5. (a) SD% and (b) UV spectra of the C-Ker-film after different contact times.

vivo to remove the excess of exudate. During swelling, water molecules start to diffuse into the network, leading to the hydration of polar hydrophilic groups and polymer extension until free water molecules and molecules within the network reach equilibrium.[48] The swelling index obtained for the C-Ker-film is 265%.

2.4. Fourier Transform Infrared (FTIR) Analysis. The study of the protein structure of the Ker-film and the C-Ker-film was performed using FTIR analysis in order to identify differences in the profile spectra. The infrared spectra of both samples are shown in Figure 6a, and they reveal the characteristic adsorption band related to the peptide bond.

https://doi.org/10.1021/acsomega.3c02525
ACS Omega 2023, 8, 30118−30128

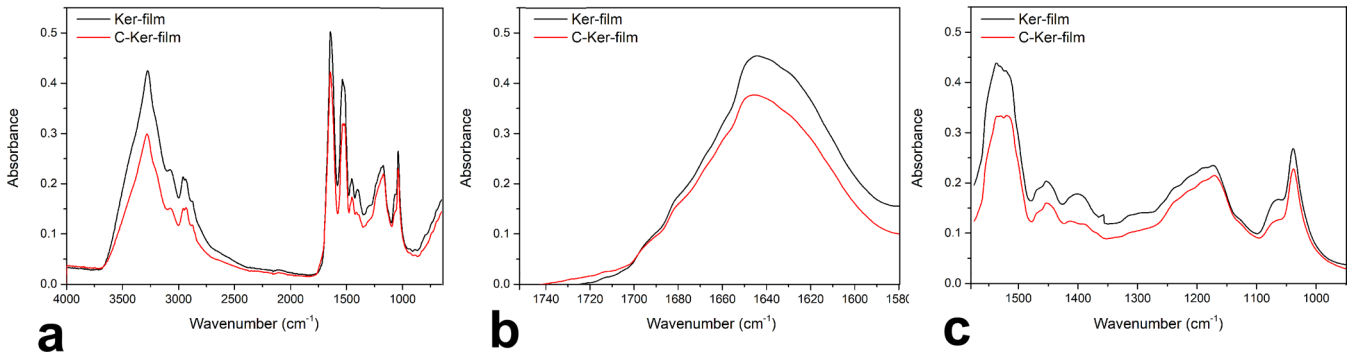

Figure 6. (a) FTIR spectra of the Ker-film and the C-Ker-film. (b) FTIR spectra between 1750 and 1580 cm^{-1} of the Ker-film and the C-Ker-film. (c) FTIR spectra between 1580 and 950 cm^{-1} of the Ker-film and the C-Ker-film.

Specifically, the band at 3282 cm^{-1} is associated with the stretching vibration of the N−H bonds (Amine A) and the band between 1700 and 1600 cm^{-1} is ascribable to the stretching vibration of the carbonyl groups (Amide I). The band between 1580 and 1510 cm^{-1} is correlated to the in-plane N−H bending and C−N stretching vibration (Amide II) and the band at 1300−1200 cm^{-1} is a complex band ascribable to Amide III. Since new peaks appear in the FTIR spectrum of the C-Ker-film, the cross-linking reaction occurred through other linkages, different from the peptide-type bond.

In order to study the structural changes induced by thermal treatment, an enlargement of Amide I and Amide II and III is reported in Figure 6b,c, respectively. In the case of the Ker-film and the C-Ker-film, no significant difference in the Amide I region between the two samples can be seen. Therefore, this excludes that the water stability can be ascribed to α-to-β transitions, as previously demonstrated by Aluigi et al.[49] On the contrary, in the region of Amide II, as shown in Figure 6c, a new peak at 1400 cm^{-1} appears in the spectra of the cross-linked keratoses related to the O−H bending of the carboxyl groups. Therefore, the C-Ker-film exhibits a more considerable amount of ester bridge based on the COOH bonds along the protein chains.[50] Furthermore, in the C-Ker-film spectrum, it is possible to observe an increased intensity of the shoulder at 1063 cm^{-1} attributed to the CO−O−CO stretching, which confirms that the cross-linking reaction occurs mainly through condensation reactions.[51] Presumably, in accordance with both the protein structure and the cross-linking temperature, it is plausible to suppose that in addition to the ester bridge, some other bonds between the acid and base groups of some amino acid side chain have occurred, mainly amide bonds, not detectable in the FTIR spectrum.

2.5. Iron Adsorption. The possible use of the C-Ker-film as a bioactive material for wound dressing was investigated. Since it was demonstrated that iron plays an essential role in chronic wound healing and based on the iron concentration in chronic wounds evaluated by Yeoh-Ellerton et al.,[20] it was decided to evaluate the binding ability of the C-Ker-film by dipping the sample into an aqueous solution of 5.85 $\mu g\ mL^{-1}$ iron (Fe^{3+}) by analyzing the iron adsorption in the function of time. Furthermore, since the average pH detected in chronic wounds is 7.6, the pH of the solution was adjusted accordingly.[52] The quantification of iron binding was performed by inductively coupled plasma-optical emission spectrometry (ICP-OES), and the results obtained were normalized according to each sample weight. The results are listed in Table 1.

Table 1. Iron Absorbed by the C-Ker-film *vs* Contact Time

time (h)	Fe^{3+} remained in solution ($\mu g\ mL^{-1}$)	Fe^{3+} adsorbed by keratoses ($\mu g\ mg^{-1}$)	Fe^{3+} adsorbed (%)
1	2.56	3.29	74%
3	1.16	4.69	80%
5	1.13	4.72	81%
12	1.13	4.72	81%
24	0.99	4.85	83%
48	0.91	4.93	84%
168	0.86	4.98	85%

Interestingly, after only one hour of contact time, the C-Ker-film is able to adsorb 3.29 $\mu g\ mg^{-1}$ iron, corresponding to 74% of the total amount. In addition, the iron-binding ability does not end after a short time, but the C-Ker-film continues the iron adsorption after 1 week of contact time, reaching 85% of the iron sequestrated.

2.6. Kinetic Studies on Iron Adsorption. Since the C-Ker-film proves to be effective in iron adsorption, the kinetic aspects have been studied in order to obtain further details about performance and mechanisms. Indeed, the kinetic parameters associated with this kind of wound dressing enable one to obtain information about the iron uptake rate and specifically the time required for completing the adsorption reaction. Therefore, the adsorption kinetics is the base to determine the performance and usage time for a future wound dressing. Thus, to investigate the possible adsorption mechanism of iron on the C-Ker-film, the pseudo-first-order and pseudo-second-order models were applied. For the pseudo-first-order model, the Lagergren equation was applied (eq 2), whereas the pseudo-second-order one was evaluated using eq 4. The fitting plots obtained by the pseudo-first-order and pseudo-second-order models are shown in Figure 7, and the kinetic parameters obtained from the two fittings are summarized in Table 2.

Regarding the pseudo-first-order data, the results are presented in Figure 7a, and the value of the constant rate k_1 was evaluated from the plot $\ln(q_e - q_t)$ *vs* t. Although the correlation coefficient is 0.998, the value of q_e is −0.4829 mg mL^{-1}, which is largely different from the experimental one. This result seems to confirm that iron adsorption onto the C-Ker-film does not follow the pseudo-first-order reaction. Similarly, the values of k_2 and q_e were evaluated by the linear plot of t/q_t *vs* t, as shown in Figure 7b. In this case, the values of k_2 and q_e were extrapolated by the intercept and the linear fit slope, respectively. In the second-order case, a good alignment

https://doi.org/10.1021/acsomega.3c02525
ACS Omega 2023, 8, 30118−30128

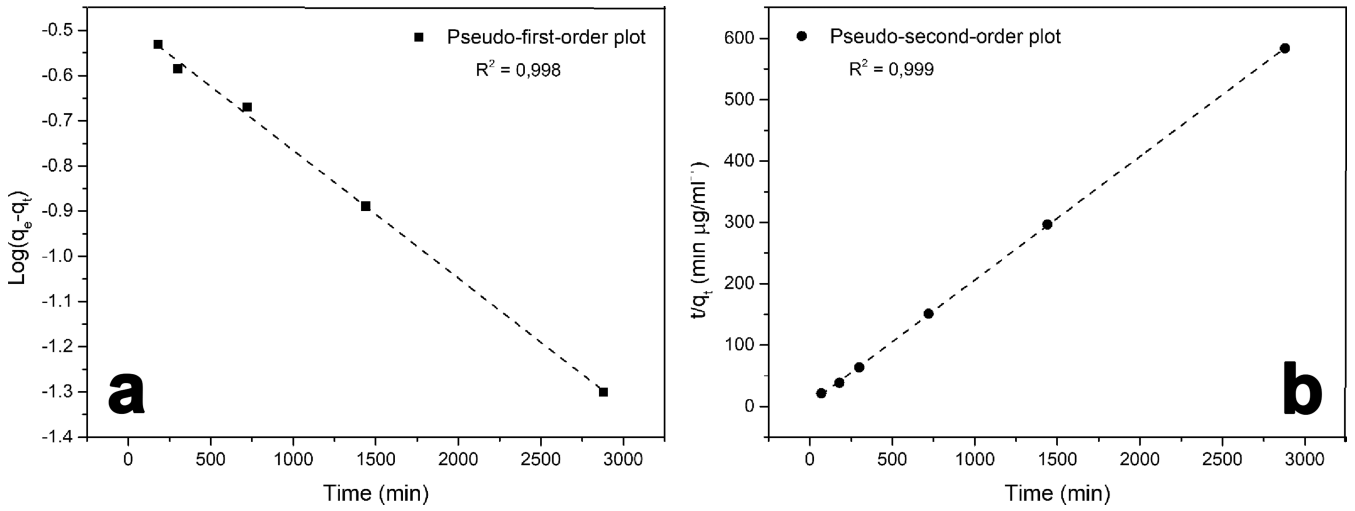

Figure 7. (a) Pseudo-first-order and (b) pseudo-second-order plots for C-Ker-film's iron adsorption.

Table 2. Kinetic and Intraparticle Diffusion Calculated Parameters

pseudo-first-order model			pseudo-second-order model		
q_e calc [mg mL^{-1}]	k_1 calc [s^{-1}]	q_e exp [mg mL^{-1}]	q_e calc [mg mL^{-1}]	k_2 calc [s^{-1}]	q_e exp [mg mL^{-1}]
−0.483	−0.0003	4.984	4.842	0.201	4.984
intraparticle diffusion					
k_{diff} [μg s$^{-1/2}$ mL^{-1}]			C		
0.0061			4.614		

between the experimental and calculated q_e values can be detected. Furthermore, the correlation coefficient (R^2) is 0.999, indicating that the pseudo-second-order kinetic is the better way to describe the adsorption mechanism of iron onto the C-Ker-film. Similar phenomena were found in keratin fibers' adsorption process.[46]

Finally, the mechanism of adsorption was investigated. Generally, the adsorption mechanism involves several steps in which the solute from the bulk solution migrates to the surface of the adsorbent, diffuses through the boundary layer, interacts with active adsorbent sites, and contributes to the diffusion phenomenon. In this case, the iron is most probably transported from the bulk of the solution into the C-Ker-film surface through the intraparticle diffusion process. Therefore, eq 5 was explored based on the intraparticle diffusion model. The evaluated plot is reported in Figure 8, and the obtained data are reported in Table 2.

Interestingly, the value of q_t was found to be linearly correlated with the values of $t^{1/2}$. The k_{diff} value is about 0.0061 μg s$^{-1/2}$ mL^{-1}, and the correlation coefficient is 0.994, indicating the good applicability of this model for describing the adsorption mechanism. Furthermore, the high intercept value seems to confirm that intraparticle diffusion is the rate-determining step since this value gives an idea about boundary-layer thickness.[53,54]

2.7. OECD QSAR: *In Silico* Approach. These results suggested testing the C-Ker-film using an *in silico* approach. These kinds of systems have gained attention since they show promising results able to replace the *in vitro* and *in vivo* methods.[55] Generally, the validity of the method is based on scientific and robust data, but in the case of complex molecules, this method leaves a certain degree of uncertainty. However, this preliminary analysis allows one to obtain good results suitable for the purpose. First, based on the results of

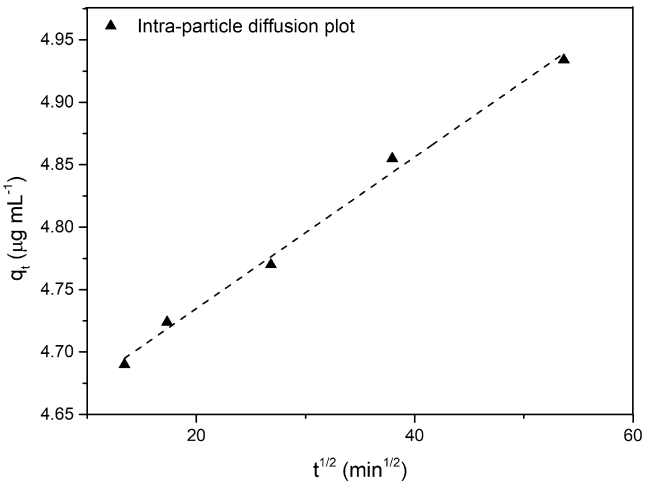

Figure 8. Intraparticle diffusion plot describing the C-Ker-film's iron adsorption.

the amino acid analysis carried out on the keratoses by Rajabinejad et al., a multicomponent compound was created to simulate the C-Ker-film structure.[44] The results are described in Table 3.

The OASIS and OECD profilers were applied to generally identify alerts for peptide reactivity. The *in chemico* DPRA approach was first investigated. Using the DPRA profilers, the QSAR Toolbox gives the results as low, moderate, or high reactivity with the Lys or Cys containing model peptides. To increase the sensitivity and negative predictive values, possible derivatives of the parent were considered. Therefore, the C-Ker-film was metabolized and all of the metabolites were analyzed taking into account the possible familiarity with other chemicals. Therefore, more than 3141 scenarios were

https://doi.org/10.1021/acsomega.3c02525
ACS Omega 2023, 8, 30118−30128

Table 3. Amino Acid Analysis on Keratosis

amino acid analysis	%mole
CYA	7.8
ASP	10.5
SER	11.6
GLU	17.7
GLY	6.7
HYS	0.5
ARG	6.0
THR	7.0
ARA	5.8
PRO	3.2
LANT	0.6
TYR	2.2
VAL	5.3
MET	0.1
LYS	3.5
ILE	2.7
LEU	7.3
PHE	1.6

processed. Interestingly, for most of the analyzed chemicals, the outcome of the profiling was "low reactivity" as DPRA results. The value obtained for KeratinoSes underlines that 12 of the 14 possible sensitizers' metabolites were classified as not sensitizer. Regarding the *in silico* test, the LLNA for guinea pig shows that the 183 possible metabolites are negative in the EC3 endpoint and therefore they could be considered as not sensitizers. The accuracy of this analysis is testified by the low number of chemicals that are considered as misclassified (3/358). These results would seem to confirm that keratin can safely be used for human applications as already tested for keratins in other forms.[37,39,43,56,57] Although *in silico* tests are very accurate, *in vitro* and *in vivo* tests still need to confirm these results.

2.8. Commercial Dressing and C-Ker Films. This last part of the results and discussion section presents a brief comparison between the materials used in chronic wound care and the proposed C-Ker-film. Usually, the dressings used for chronic wound healing are made of different materials and shapes. Thus, the dressings typically used are various, such as films, gauze, hydrogels, hydrocolloid foam, and silver- and alginate-based bandages. All of these dressings are suitable for removing the exudate and protecting the wound from infection. These dressings are generally left on the injury for several days. After that, the dressing needs be changed, causing pain and wasting patient time. It is estimated that over 8.2 million people suffer from chronic wounds, and the cost related to their treatments would be between 28 and 96 billion dollars.[58] The first type of chronic wound dressing was made of natural fenestration such as Vaseline or cotton bandages.[59] This kind of treatment is easy to use and often already accessible, but once they are saturated with exudate, they quickly lose their efficacy.[60] Thus, they are often impregnated with hydrophobic coatings such as petroleum jelly and waxes to increase their durability and their liquid resistance. Modern dressings are more focused on the environmental wound problem, and therefore, the bandages are generally enriched with compounds that contain growth factors able to increase angiogenesis and decrease fibrosis.[61] The four classic dressing types are foam, hydrocolloid, hydrogels, and films. Since they are actually used, all of these bandages often contain some drawbacks; for example, they are difficult to be removed, disturbing the new keratocytes, requiring secondary dressings, and causing the maceration of the skin around the wound. Based on these considerations, it is necessary to find alternative solutions, creating a dressing able to form a barrier for the trauma, promoting a patient's quality of life, reducing pain, frequent bandage changes, and scar tissue formation. Considering this, keratin-based materials seem to be suitable alternatives since they have been proven to have good bioactivity, biocompatibility, and biodegradability.

Furthermore, keratin is one of the most abundant natural compounds and therefore it is an easily available material.[56] Finally, keratins have been widely developed in hemostasis and wound-healing applications.[57] For example, Yang et al. successfully used keratin-based hydrogels from chicken feathers for chronic wound care.[62] The *in vivo* studies showed that keratin hydrogels could be used for biomedical applications, especially in promoting effective wound healing. Another work demonstrates that the prepared novel bionic keratin-bilayer wound dressing could promote cell growth and the excellent swelling properties could quickly absorb wound exudate and create an environment suitable for the healing process.[63] Taking into account all of these considerations, the C-Ker-films fall into that segment of the market that currently requires the use of new, efficient, and natural materials and could be viable replacements for current methods of chronic wound care. Indeed, this material seems to possess all of the suitable characteristics to be exploited for biomedical treatments. Certainly, the C-Ker-film combines the iron-binding ability, responsible for prolonging the oxidative phase in a chronic wound, with its ability to swell and therefore to remove exudate from wounds. Preliminary experiments conducted in water show that although the structure can absorb a large amount of water, it does not have any influence on the capacity of this material to act as a radical scavenger even after more than a week of use. In addition, this material can be prepared from waste materials, making it both economically and environmentally valuable.

3. CONCLUSIONS AND PROSPECTS

A soluble keratose film was successfully obtained by casting, and the resulting film was defect-free, homogeneous, and transparent. After a simple thermal treatment at 170 °C for 30 min, the films become perfectly insoluble with high water stability for up to 1 week. The TGA and FTIR analyses demonstrate that the cross-linking reaction occurs mainly through the protein chain's acid and basic groups. No modification can be detected in the Amide I spectra, indicating that the α-to-β transition does not occur during the thermal treatment. The possibility of using the C-Ker-film for removing iron in the chronic wound was confirmed and evaluated by testing the Fe^{3+} adsorption. The ICP-OES data demonstrate that the C-Ker-film was able to bind 83% of iron after only 24 h and 85% after 1 week. The iron adsorption proceeds mainly through a pseudo-second-order kinetics, and the intraparticle diffusion model seems to be able to describe the adsorption mechanism. The high swelling ability of the C-Ker-film, its outstanding biocompatibility, and its capacity to absorb one of the principals responsible for the oxidative reactions that prevent proper wound healing suggest that research should move toward *in vitro* and *in vivo* studies in order to develop a wound dressing with an excellent healing effect. Since the C-Ker-film is a new and complex material, further analysis, such

https://doi.org/10.1021/acsomega.3c02525
ACS Omega 2023, 8, 30118−30128

as cytotoxicity and wound environment stability, must be performed. Nevertheless, these encouraging data and the results of these preliminary *in silico* tests seem to confirm the possible application of this new biomaterial as a bioactive wound dressing reducing the iron concentration, decreasing the radical scavenger activity and finally supporting wound healing.

4. EXPERIMENTAL SECTION

4.1. Materials. Wool was kindly provided by the Biella textile company (Italy). Peracetic acid, hydrochloric acid, Fe_2Cl_3, tris(hydroxymethyl)aminomethane (Tris), dichloromethane, nitric acid, and ethanol were purchased from Sigma Aldrich. The iron standard for ICP TraceCERT, 1000 mg L^{-1} in nitric acid (Perkin-Elmer), was used to calibrate inductively coupled plasma-optical emission spectroscopy (ICP-OES). Wool was extracted in Soxhlet with dichloromethane and ethanol for 4 h, dried in an oven at 105 °C until constant weight, and finally conditioned for 24 h (20 °C, 65% R.H.).

4.2. Keratose Extraction. The oxidative procedure was applied for keratose extraction, as reported in the literature.[44] Briefly, wool (4 g) was dipped in a solution containing 2% peracetic acid (36−40% peracetic acid in an acetic acid solution) with a fiber-to-liquor ratio of 1:50 for 24 h at room temperature. Actually, 4 g of wool was dipped in 200 mL of peracetic acid in a flash. The solution was then placed in a thermostatic bath and stirred for 24 h. After that, the solution was filtered using a 120-mesh sieve, rinsed with MilliQ water, and dried at 20 °C for 24 h. Then, the sample was treated in a Linitest apparatus with a solution of Tris (1 M) solution for 2 h at 37 °C. Precisely, 1 g of wool treated with peracetic acid is placed inside a test tube and placed in contact with 10 mL of Tris 1 molar. After that, the tubes are placed inside a sleeve and positioned in the Linitest. The solution was then filtered with a 120-mesh sieve, and the pH was adjusted to 7 with HCl (1 M). The filtrate was dialyzed in a cellulose tube (molecular weight cutoff 12−14 kDa) in a distilled water-circulated system for one day. The obtained keratoses were then freeze-dried.

The extraction yield of the protein from the wool sample was evaluated using the following equation

$$Y(\%) = \frac{W_e}{W_w} \quad (1)$$

where Y (%) is the yield, W_e is the dry weight of extracted keratoses obtained after freeze-drying, and W_w is the initial weight of the wool.

4.3. Preparation of Keratose Film (Ker-film) and Self-Cross-Linked Keratose Film (C-Ker-film). The keratose film was prepared by dissolving 0.1896 g in 2 mL of MilliQ water and stirred for 10 min at room temperature in closed vials. Then, the solution was poured into a polypropylene mold, and the solvent was allowed to evaporate at 20 °C for 48 h. After that, the films were removed from the mold, put in a ceramic crucible, and cured in a static oven at 170 °C for 1 h to obtain the insoluble C-Ker-film.

4.4. Characterization. *4.4.1. FTIR Analysis.* The FTIR spectra of the Ker-film and the C-Ker-film were collected with the smart endurance attenuated total reflection (ATR) technique in the range from 4000 to 650 cm^{-1} with 64 scans and 4 cm^{-1} of resolution through a Thermo Nicolet Nexus IZ10 (Milan, Italy) spectrometer equipped with ZnSe single-crystal reflection with Ominc as software.

4.4.2. Thermal Analyses. Thermogravimetric analyses were carried out in a TGA Mettler Toledo (Columbus, Ohio), with a STARe system under a nitrogen atmosphere (gas flux 100 mL min^{-1}). The sample (about 10 mg) was placed in an alumina open pan and heated to 800 °C by a ramping temperature of 10 °C min^{-1} under a nitrogen flow.

Differential scanning calorimetry (DSC) analyses were performed with a Mettler TA 3000 apparatus (Mattler-Toledo, Columbus, Ohio) and STARe software equipped with a DSC 20 cell purged with nitrogen. The Ker-film was studied in a heat−cool−heat cycle in the range from 30 to 195 °C with a ramp rate of 10 °C min^{-1}, under 50 mL of nitrogen flow. The curing process was studied by an isothermal step at 170 °C, followed by cooling to 30 °C and then a second heating ramp to assess the curing process.

4.4.3. Water Adsorption and Stability. The water stability was evaluated by dipping the samples in water at room temperature for a variable time, ranging from 1 h to 2 weeks, and the stability degree (S.D.) was evaluated as follows

$$SD(\%) = {W_{s2}}/{W_{s1}} \times 100 \quad (2)$$

The weight of the sample before (W_{s1}) and after dipping it (W_{s2}) was evaluated. The water solutions were also analyzed with a double-bean Perkin-Elmer 200 UV−vis spectrophotometer at 270 nm. Indeed, before the cross-linking treatment, the Ker-film was perfectly soluble in water, generating an absorption band at 270 cm^{-1} in the UV−vis spectra. Thus, the cured films were dipped in water and the supernatant was evaluated after different contact times (specifically, after 1, 3, 5, 12, 24, 48 h, and 1 week) in order to check the presence of the absorption band at 270 cm^{-1}.

The swelling test was evaluated by calculating the weight of the material after the water adsorption *vs* the weight of the dry material (W_{gel}/W_{dry}). Specifically, W_{gel} is the weight of the gel at swelling maximum and W_{dry} is the weight of the dried gel. The swelling experiments were conducted by immersing the C-Ker-film (500 mg) in different water volumes until the water was not already adsorbed at RT. After that, the sample was measured and the weight was recorded.

4.5. Iron Adsorption Evaluation. Iron adsorption was quantified by inductively coupled plasma-optical emission spectroscopy, ICP OPTIMA 7000 equipped with WinLan 32 software (Perkin-Elmer, Milan, Italy). The ICP was equipped with a cyclonic spray chamber and a Teflon Mira Mist nebulizer. The instrumental conditions were plasma power 1.5 kW; sample aspiration rate 15 rpm (∼2 mL min^{-1}); argon nebulizer flow 0.6 L min^{-1}; argon auxiliary flow 0.2 L min^{-1}; and argon plasma flow 15 L min^{-1}.

The adsorption experiments were performed starting from 50 mL of a 5.85 ppm Fe^{3+} aqueous solution, the concentration of iron detected in chronic wounds in the literature.[20] The pH of the solutions was adjusted to 7.6 with HCl 1 M. The adsorption experiments were carried out at room temperature by dipping 2 mg of C-Ker-film for different times ranging from 1 to 168 h (1 week). ICP-OES analysis was performed by previously filtering the solution with a PTFE filter (0.45 μm) and then adding 1% v/v nitric acid (65% wt). Each concentration value was averaged based on three measurements. ICP-OES data are expressed in μg mg^{-1}.

4.6. Kinetic and Adsorption Studies. The kinetic and adsorption parameters associated with iron adsorption were evaluated using different models. Specifically, the adsorption

https://doi.org/10.1021/acsomega.3c02525
ACS Omega 2023, 8, 30118−30128

data collected by analyzing the supernatants after different exposure times (specifically, after 1, 3, 5, 12, 24, 48 h, and 1 week) of the C-Ker-film with 5.85 ppm iron were analyzed using two kinetic models: pseudo-first-order and pseudo-second-order kinetic. The pseudo-first-order equation used is the following[45]

$$\log(q_e - q_t) = \log\ q_e - \left(\frac{k_1}{2.303}\right)t \quad (3)$$

where the amounts of iron (mg g^{-1}) adsorbed on the C-Ker-film at equilibrium and at time t are expressed as q_e and q_t, respectively. The pseudo-first-order rate constant, k_1 (min^{-1}), was obtained from the slope of the linear plots of $\log(q_e - q_t)$ *vs* t.

For the pseudo-second-order mechanism, the data were elaborated as follows[45,46]

$$t/q_t = (1/h) + (1/q_e)t \quad (4)$$

Here, q_e and q_t are amounts of iron (mg g^{-1}) adsorbed on the C-Ker-film at equilibrium and at time t, respectively, and h represents the initial rate of adsorption (mg g^{-1} min) and is given by

$$h = k_2 q_e^2 \quad (5)$$

where k_2 is the rate constant of the pseudo-second-order adsorption (mg g^{-1} min), and it was determined by the linear plot of t/q_t against t.

Furthermore, the iron adsorption mechanism was evaluated, calculating the interparticle diffusion model, which was determined by using eq 6.

$$q_t = k_{diff}t + C \quad (6)$$

where C is the intercept and k_{dif} is the intraparticle diffusion rate constant (mol $min^{-1/2}$ g^{-1}).

4.7. QSAR Toolbox. To obtain information about the possible chemical and physical interactions of the C-Ker-film, the OECD QSAR Toolbox v4.0 (*Echa*) was applied. The OECD QSAR Toolbox is a software designed to support hazard assessment of chemicals and increase knowledge cost-efficiently. Actually, for this analysis, the keratosis structure was assimilated into the keratin structure and analyzed. Since the software has a huge database, some critical parameters were explored by profiling the structure. Briefly, the toxicological mechanism assumed to be responsible for the effect is assigned to the C-Ker-film. In this case, the protein binding interactions were supposed to be the main toxicity mechanisms. Furthermore, for the C-Ker-film, the possible effect related to the generation of metabolites resulting from enzymatic activities was also considered.

The two profilers, "Protein binding by OASIS" and "Protein binding by OECD", were selected for this study. Then, for the C-Ker-films, skin metabolites were generated and then those were profiled for protein binding alerts. The QSAR Toolbox was used to subcategorize and fill the gaps in terms of structural similarity, and skin sensitization in humans was used as the endpoint. The first data input for this analysis was the Direct Peptide Reactivity Assay (DPRA). DPRA is an *in chemico* test that measures the reactivity of a test substance toward two model synthetic peptides, one containing lysine and the other containing cysteine.[47] Then, the KeratinoSens test method was applied. This process assesses the ability of substances to activate cytokines and induce cytoprotective genes in keratinocytes.[47] Finally, *in silico* predictions were made by LLNA, guinea pig, and human outcomes. These analysis results can be approximated as: −alert present ≡ skin sensitizer; −no alert present ≡ nonsensitizer. Therefore, the results of these predictions were considered for obtaining some preliminary data about the possible *in vivo* behavior of the C-Ker-film.

AUTHOR INFORMATION

Corresponding Author

Alessia Patrucco − *CNR-STIIMA, Italian National Research Council, Institute of Intelligent Industrial Technologies and Systems for Advanced Manufacturing, 13900 Biella, Italy;* orcid.org/0000-0002-6105-0226; Email: alessia.patrucco@stiima.cnr.it

Authors

Anastasia Anceschi − *CNR-STIIMA, Italian National Research Council, Institute of Intelligent Industrial Technologies and Systems for Advanced Manufacturing, 13900 Biella, Italy*

Parag Bhavsar − *CNR-STIIMA, Italian National Research Council, Institute of Intelligent Industrial Technologies and Systems for Advanced Manufacturing, 13900 Biella, Italy*

Marina Zoccola − *CNR-STIIMA, Italian National Research Council, Institute of Intelligent Industrial Technologies and Systems for Advanced Manufacturing, 13900 Biella, Italy;* orcid.org/0000-0002-5356-4817

Mirko Tessari − *Vascular Diseases Center, University of Ferrara, 44121 Ferrara, Italy*

Luca Erbazzi − *Vascular Diseases Center, University of Ferrara, 44121 Ferrara, Italy*

Paolo Zamboni − *Vascular Diseases Center, University of Ferrara, 44121 Ferrara, Italy*

Complete contact information is available at: https://pubs.acs.org/10.1021/acsomega.3c02525

Notes

The authors declare no competing financial interest.

ACKNOWLEDGMENTS

The authors wish to thank the supervisors for their contribution and other colleagues for their valuable technical support on this project.

REFERENCES

(1) Vos, T.; et al. Global, Regional, and National Incidence, Prevalence, and Years Lived with Disability for 301 Acute and Chronic Diseases and Injuries in 188 Countries, 1990−2013: A Systematic Analysis for the Global Burden of Disease Study 2013. *Lancet* **2015**, *386*, 743−800.

(2) Frykberg, R. G.; Banks, J. Challenges in the Treatment of Chronic Wounds. *Adv. Wound Care* **2015**, *4*, 560−582.

(3) Spampinato, S. F.; Caruso, G. I.; De Pasquale, R.; Sortino, M. A.; Merlo, S. The Treatment of Impaired Wound Healing in Diabetes: Looking among Old Drugs. *Pharmaceuticals* **2020**, *13*, No. 60.

(4) Tomic, D.; Shaw, J. E.; Magliano, D. J. The Burden and Risks of Emerging Complications of Diabetes Mellitus. *Nat. Rev. Endocrinol.* **2022**, *18*, 525−539.

(5) Rice, J. B.; Desai, U.; Cummings, A. K. G.; Birnbaum, H. G.; Skornicki, M.; Parsons, N. B. Burden of Diabetic Foot Ulcers for Medicare and Private Insurers. *Diabetes Care* **2014**, *37*, 651−658.

https://doi.org/10.1021/acsomega.3c02525
ACS Omega 2023, 8, 30118−30128

(6) De Mattei, M.; Ongaro, A.; Magaldi, S.; Gemmati, D.; Legnaro, A.; Palazzo, A.; Masieri, F.; Pellati, A.; Catozzi, L.; Caruso, A.; Zamboni, P. Time- and Dose-Dependent Effects of Chronic Wound Fluid on Human Adult Dermal Fibroblasts. *Dermatol. Surg.* **2008**, *34*, 347−356.
(7) Sim, S. L.; Kumari, S.; Kaur, S.; Khosrotehrani, K. Macrophages in Skin Wounds: Functions and Therapeutic Potential. *Biomolecules* **2022**, *12*, No. 1659.
(8) Wei, X.; Li, M.; Zheng, Z.; Ma, J.; Gao, Y.; Chen, L.; Peng, Y.; Yu, S.; Yang, L. Senescence in Chronic Wounds and Potential Targeted Therapies. *Burns Trauma* **2022**, *10*, No. tkab045.
(9) Zamboni, P.; Lanzara, S.; Mascoli, F.; Caggiati, A.; Liboni, A. Inflammation in venous disease Review. *Int. Angiol.* **2008**, *27*, 361−369.
(10) Zamboni, P.; De Mattei, M.; Ongaro, A.; Fogato, L.; Carandina, S.; De Palma, M.; Tognazzo, S.; Scapoli, G. L.; Serino, M. L.; Caruso, A.; Liboni, A.; Gemmati, D. Factor XIII Contrasts the Effects of Metalloproteinases in Human Dermal Fibroblast Cultured Cells. *Vasc. Endovascular Surg.* **2004**, *38*, 431−438.
(11) Uttara, B.; Singh, A. V.; Zamboni, P.; Mahajan, R. T. Oxidative Stress and Neurodegenerative Diseases: A Review of Upstream and Downstream Antioxidant Therapeutic Options. *Curr. Neuropharmacol.* **2009**, *7*, 65−74.
(12) Singh, A. V.; Subhashree, L.; Milani, P.; Gemmati, D.; Zamboni, P. Interplay of Iron Metallobiology, Metalloproteinases, and FXIII, and Role of Their Gene Variants in Venous Leg Ulcer. *Int. J. Low. Extrem. Wounds* **2010**, *9*, 166−179.
(13) Timoshnikov, V. A.; Selyutina, O. Y.; Polyakov, N. E.; Didichenko, V.; Kontoghiorghes, G. J. Mechanistic Insights of Chelator Complexes with Essential Transition Metals: Antioxidant/Pro-Oxidant Activity and Applications in Medicine. *Int. J. Mol. Sci.* **2022**, *23*, No. 1247.
(14) Wright, J. A.; Richards, T.; Srai, S. K. The Role of Iron in the Skin and Cutaneous Wound Healing. *Front. Pharmacol.* **2014**, *5*, 156.
(15) Myers, H. L. Topical Chelation Therapy for Varicose Pigmentation. *Angiology* **1966**, *17*, 66−68.
(16) Ackerman, Z.; Seidenbaum, M.; Loewenthal, E.; Rubinow, A. Overload of Iron in the Skin of Patients With Varicose Ulcers: Possible Contributing Role of Iron Accumulation in Progression of the Disease. *Arch. Dermatol.* **1988**, *124*, 1376−1378.
(17) Wang, X.; Fan, D.; Cao, X.; Ye, Q.; Wang, Q.; Zhang, M.; Xiao, C. The Role of Reactive Oxygen Species in the Rheumatoid Arthritis-Associated Synovial Microenvironment. *Antioxidants* **2022**, *11*, No. 1153.
(18) Ferris, A. E.; Harding, K. G. An Overview of the Relationship between Anaemia, Iron, and Venous Leg Ulcers. *Int. Wound J.* **2019**, *16*, 1323−1329.
(19) Wlaschek, M.; Singh, K.; Sindrilaru, A.; Crisan, D.; Scharffetter-Kochanek, K. Iron and Iron-Dependent Reactive Oxygen Species in the Regulation of Macrophages and Fibroblasts in Non-Healing Chronic Wounds. *Free Radical Biol. Med.* **2019**, *133*, 262−275.
(20) Yeoh-Ellerton, S.; Stacey, M. C. Iron and 8-Isoprostane Levels in Acute and Chronic Wounds. *J. Invest. Dermatol.* **2003**, *121*, 918−925.
(21) Zamboni, P.; Tognazzo, S.; Izzo, M.; Pancaldi, F.; Scapoli, G. L.; Liboni, A.; Gemmati, D. Hemochromatosis C282Y Gene Mutation Increases the Risk of Venous Leg Ulceration. *J. Vasc. Surg.* **2005**, *42*, 309−314.
(22) Suarato, G.; Bertorelli, R.; Athanassiou, A. Borrowing From Nature: Biopolymers and Biocomposites as Smart Wound Care Materials. *Bioeng. Biotechnol* **2018**, *6*, No. 137.
(23) Pereira, R. F.; Barrias, C. C.; Granja, P. L.; Bartolo, P. J. Advanced Biofabrication Strategies for Skin Regeneration and Repair. *Nanomedicine* **2013**, *8*, 603−621.
(24) Bloise, N.; Patrucco, A.; Bruni, G.; Montagna, G.; Caringella, R.; Fassina, L.; Tonin, C.; Visai, L. In Vitro Production of Calcified Bone Matrix onto Wool Keratin Scaffolds via Osteogenic Factors and Electromagnetic Stimulus. *Materials* **2020**, *13*, No. 3052.
(25) Varan, C.; Anceschi, A.; Sevli, S.; Bruni, N.; Giraudo, L.; Bilgiç, E.; Korkusuz, P.; İskit, A. B.; Trotta, F.; Bilensoy, E. Preparation and Characterization of Cyclodextrin Nanosponges for Organic Toxic Molecule Removal. *Int. J. Pharm.* **2020**, *585*, No. 119485.
(26) Azimi, B.; Maleki, H.; Zavagna, L.; De la Ossa, J. G.; Linari, S.; Lazzeri, A.; Danti, S. Bio-Based Electrospun Fibers for Wound Healing. *J. Funct. Biomater.* **2020**, *11*, No. 67.
(27) Tenorová, K.; Masteiková, R.; Pavloková, S.; Kostelanská, K.; Bernatonienė, J.; Vetchý, D. Formulation and Evaluation of Novel Film Wound Dressing Based on Collagen/Microfibrillated Carboxymethylcellulose Blend. *Pharmaceutics* **2022**, *14*, No. 782.
(28) Singh, A. V.; Gemmati, D.; Kanase, A.; Pandey, I.; Misra, V.; Kishore, V.; Jahnke, T.; Bill, J. Nanobiomaterials for Vascular Biology and Wound Management: A Review *Veins Lymphatics* 2018; Vol. 7 2 DOI: 10.4081/vl.2018.7196.
(29) Yoon, D.; Yoon, D.; Cha, H. J.; Lee, J. S.; Chun, W. Enhancement of Wound Healing Efficiency Mediated by Artificial Dermis Functionalized with EGF or NRG1. *Biomed. Mater.* **2018**, *13*, No. 045007.
(30) Ghica, M. V.; Albu Kaya, M. G.; Dinu-Pîrvu, C.-E.; Lupuleasa, D.; Udeanu, D. I. Development, Optimization and In Vitro/In Vivo Characterization of Collagen-Dextran Spongious Wound Dressings Loaded with Flufenamic Acid. *Molecules* **2017**, *22*, No. 1552.
(31) Guo, R.; Lan, Y.; Xue, W.; Cheng, B.; Zhang, Y.; Wang, C.; Ramakrishna, S. Collagen-Cellulose Nanocrystal Scaffolds Containing Curcumin-Loaded Microspheres on Infected Full-Thickness Burns Repair. *J. Tissue Eng. Regen. Med.* **2017**, *11*, 3544−3555.
(32) Bhowmick, S.; Thanusha, A. V.; Kumar, A.; Scharnweber, D.; Rother, S.; Koul, V. Nanofibrous Artificial Skin Substitute Composed of MPEG-PCL Grafted Gelatin/Hyaluronan/Chondroitin Sulfate/Sericin for 2nd Degree Burn Care:: In Vitro and in Vivo Study. *RSC Adv.* **2018**, *8*, 16420−16432.
(33) Caringella, R.; Bhavsar, P.; Dalla Fontana, G.; Patrucco, A.; Tonin, C.; Pozzo, P. D.; Zoccola, M. Fabrication and Properties of Keratoses/Sericin Blend Films. *Polym. Bull.* **2022**, *79*, 2189−2204.
(34) Reimers, K.; Liebsch, C.; Radtke, C.; Kuhbier, J. W.; Vogt, P. M. Silks as Scaffolds for Skin Reconstruction. *Biotechnol. Bioeng.* **2015**, *112*, 2201−2205.
(35) Bragulla, H. H.; Homberger, D. G. Structure and Functions of Keratin Proteins in Simple, Stratified, Keratinized and Cornified Epithelia. *J. Anat.* **2009**, *214*, 516−559.
(36) Fortunato, G. M.; Da Ros, F.; Bisconti, S.; De Acutis, A.; Biagini, F.; Lapomarda, A.; Magliaro, C.; De Maria, C.; Montemurro, F.; Bizzotto, D.; Braghetta, P.; Vozzi, G. Electrospun Structures Made of a Hydrolyzed Keratin-Based Biomaterial for Development of in Vitro Tissue Models. *Front. Bioeng. Biotechnol.* **2019**, *7*, 174.
(37) Tachibana, A.; Furuta, Y.; Takeshima, H.; Tanabe, T.; Yamauchi, K. Fabrication of Wool Keratin Sponge Scaffolds for Long-Term Cell Cultivation. *J. Biotechnol.* **2002**, *93*, 165−170.
(38) Tonin, C.; Zoccola, M.; Aluigi, A.; Varesano, A.; Montarsolo, A.; Vineis, C.; Zimbardi, F. Study on the Conversion of Wool Keratin by Steam Explosion. *Biomacromolecules* **2006**, *7*, 3499−3504.
(39) Su, C.; Gong, J.-S.; Ye, J.-P.; He, J.-M.; Li, R.-Y.; Jiang, M.; Geng, Y.; Zhang, Y.; Chen, J.-H.; Xu, Z.-H.; Shi, J.-S. Enzymatic Extraction of Bioactive and Self-Assembling Wool Keratin for Biomedical Applications. *Macromol. Biosci.* **2020**, *20*, No. 2000073.
(40) Ji, Y.; Chen, J.; Lv, J.; Li, Z.; Xing, L.; Ding, S. Extraction of Keratin with Ionic Liquids from Poultry Feather. *Sep. Purif. Technol.* **2014**, *132*, 577−583.
(41) Pakkaner, E.; Yalçın, D.; Uysal, B.; Top, A. Self-Assembly Behavior of the Keratose Proteins Extracted from Oxidized Ovis Aries Wool Fibers. *Int. J. Biol. Macromol.* **2019**, *125*, 1008−1015.
(42) Sando, L.; Kim, M.; Colgrave, M. L.; Ramshaw, J. A.; Werkmeister, J. A.; Elvin, C. M. Photochemical Crosslinking of Soluble Wool Keratins Produces a Mechanically Stable Biomaterial That Supports Cell Adhesion and Proliferation. *J. Biomed. Mater. Res., Part A* **2010**, *95*, 901−911.

https://doi.org/10.1021/acsomega.3c02525
ACS Omega 2023, 8, 30118−30128

(43) Ledford, B.; Barron, C.; Van Dyke, M.; He, J.-Q. Keratose Hydrogel for Tissue Regeneration and Drug Delivery. *Semin. Cell Dev. Biol.* **2022**, *128*, 145−153.
(44) Rajabinejad, H.; Zoccola, M.; Patrucco, A.; Montarsolo, A.; Rovero, G.; Tonin, C. Physicochemical Properties of Keratin Extracted from Wool by Various Methods. *Text. Res. J.* **2018**, *88*, 2415−2424.
(45) Revellame, E. D.; Fortela, D. L.; Sharp, W.; Hernandez, R.; Zappi, M. E. Adsorption Kinetic Modeling Using Pseudo-First Order and Pseudo-Second Order Rate Laws: A Review. *Cleaner Eng. Technol.* **2020**, *1*, No. 100032.
(46) Anceschi, A.; Zoccola, M.; Mossotti, R.; Bhavsar, P.; Dalla Fontana, G.; Patrucco, A. Colorimetric Quantification of Virgin and Recycled Cashmere Fibers: Equilibrium, Kinetic, and Thermodynamic Studies. *J. Nat. Fibers* **2022**, *19*, 11064−11077.
(47) Strickland, J.; Zang, Q.; Kleinstreuer, N.; Paris, M.; Lehmann, D. M.; Choksi, N.; Matheson, J.; Jacobs, A.; Lowit, A.; Allen, D.; Casey, W. Integrated Decision Strategies for Skin Sensitization Hazard. *J. Appl. Toxicol.* **2016**, *36*, 1150−1162.
(48) Singh, A. V.; Kayal, A.; Malik, A.; Maharjan, R. S.; Dietrich, P.; Thissen, A.; Siewert, K.; Curato, C.; Pande, K.; Prahlad, D.; Kulkarni, N.; Laux, P.; Luch, A. Interfacial Water in the SARS Spike Protein: Investigating the Interaction with Human ACE2 Receptor and In Vitro Uptake in A549 Cells. *Langmuir* **2022**, *38*, 7976−7988.
(49) Aluigi, A.; Corbellini, A.; Rombaldoni, F.; Zoccola, M.; Canetti, M. Morphological and Structural Investigation of Wool-Derived Keratin Nanofibres Crosslinked by Thermal Treatment. *Int. J. Biol. Macromol.* **2013**, *57*, 30−37.
(50) Anceschi, A.; Magnacca, G.; Trotta, F.; Zanetti, M. Preparation and Characterization of Microporous Carbon Spheres from High Amylose Pea Maltodextrin. *RSC Adv.* **2017**, *7*, 36117−36123.
(51) Singh, A. V.; Jahnke, T.; Kishore, V.; Park, B.-W.; Batuwangala, M.; Bill, J.; Sitti, M. Cancer Cells Biomineralize Ionic Gold into Nanoparticles-Microplates via Secreting Defense Proteins with Specific Gold-Binding Peptides. *Acta Biomater.* **2018**, *71*, 61−71.
(52) Derwin, R.; Patton, D.; Strapp, H.; Moore, Z. Wound PH and Temperature as Predictors of Healing: An Observational Study. *J. Wound Care* **2023**, *32*, 302−310.
(53) Pellicer, J. A.; Rodríguez-López, M. I.; Fortea, M. I.; Lucas-Abellán, C.; Mercader-Ros, M. T.; López-Miranda, S.; Gómez-López, V. M.; Semeraro, P.; Cosma, P.; Fini, P.; Franco, E.; Ferrándiz, M.; Pérez, E.; Ferrándiz, M.; Núñez-Delicado, E.; Gabaldón, J. A. Adsorption Properties of β- and Hydroxypropyl-β-Cyclodextrins Cross-Linked with Epichlorohydrin in Aqueous Solution. A Sustainable Recycling Strategy in Textile Dyeing Process. *Polymers* **2019**, *11*, No. 252.
(54) Doğan, M.; Alkan, M.; Türkyilmaz, A.; Özdemir, Y. Kinetics and Mechanism of Removal of Methylene Blue by Adsorption onto Perlite. *J. Hazard. Mater.* **2004**, *109*, 141−148.
(55) Benigni, R.; Bassan, A.; Pavan, M. In Silico Models for Genotoxicity and Drug Regulation. *Expert Opin. Drug Metab. Toxicol.* **2020**, *16*, 651−662.
(56) Yan, R.-R.; Gong, J.-S.; Su, C.; Liu, Y.-L.; Qian, J.-Y.; Xu, Z.-H.; Shi, J.-S. Preparation and Applications of Keratin Biomaterials from Natural Keratin Wastes. *Appl. Microbiol. Biotechnol.* **2022**, *106*, 2349−2366.
(57) Dickerson, M. B.; Sierra, A. A.; Bedford, N. M.; Lyon, W. J.; Gruner, W. E.; Mirau, P. A.; Naik, R. R. Keratin-Based Antimicrobial Textiles{,} Films{,} and Nanofibers. *J. Mater. Chem. B* **2013**, *1*, 5505−5514.
(58) Https://essentialhh.org/how-much-does-wound-care-cost-il/. How much does care cost? https://www.payingforcare.org/how-much-does-care-cost.
(59) Powers, J. G.; Morton, L. M.; Phillips, T. J. Dressings for Chronic Wounds. *Dermatol. Ther.* **2013**, *26*, 197−206.
(60) Nuutila, K.; Eriksson, E. Moist Wound Healing with Commonly Available Dressings. *Adv. Wound Care* **2021**, *10*, 685−698.
(61) Deng, X.; Gould, M.; Ali, M. A. A Review of Current Advancements for Wound Healing: Biomaterial Applications and Medical Devices. *J. Biomed. Mater. Res., Part B* **2022**, *110*, 2542−2573.
(62) Wang, J.; Hao, S.; Luo, T.; Cheng, Z.; Li, W.; Gao, F.; Guo, T.; Gong, Y.; Wang, B. Feather Keratin Hydrogel for Wound Repair: Preparation, Healing Effect and Biocompatibility Evaluation. *Colloids Surf., B* **2017**, *149*, 341−350.
(63) Zhang, M.; Xu, S.; Du, C.; Wang, R.; Han, C.; Che, Y.; Feng, W.; Wang, C.; Gao, S.; Zhao, W. Novel PLCL Nanofibrous/Keratin Hydrogel Bilayer Wound Dressing for Skin Wound Repair. *Colloids Surf., B* **2023**, *222*, No. 113119.

https://doi.org/10.1021/acsomega.3c02525
ACS Omega 2023, 8, 30118−30128